Cell Reports, Volume *18*

Supplemental Information

Measurement of Rapid Protein Diffusion in the Cytoplasm by Photo-Converted Intensity Profile Expansion

Rotem Gura Sadovsky, Shlomi Brielle, Daniel Kaganovich, and Jeremy L. England

Supplemental items

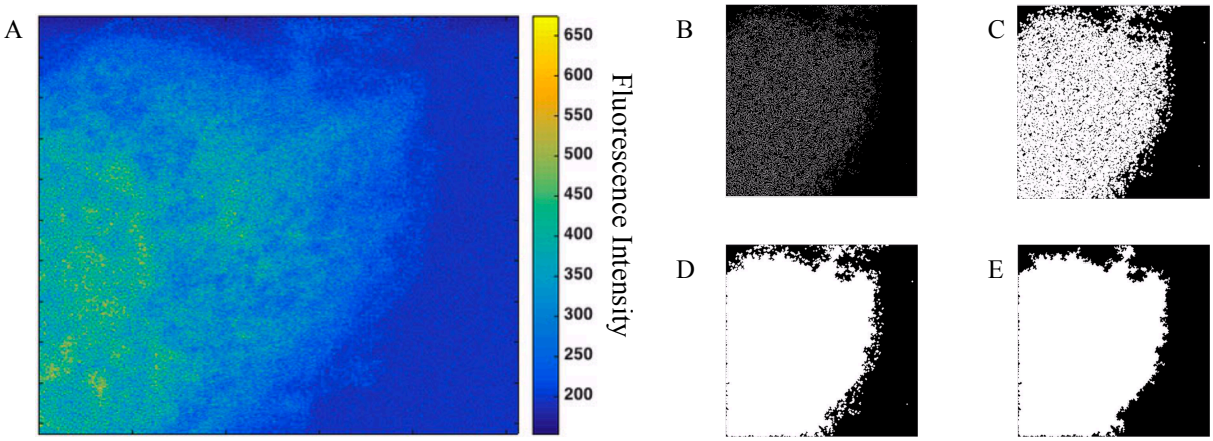

Figure S1. Related to Figure 1. The image segmentation process. A) The average of the first 30 images of a typical photo-conversion movie is shown as a heat map of fluorescence intensity. B-E) The cell mask is shown at different stages of the analysis: B) after edge detection, C) after dilation, D) after hole filling, and E) after erosion and selection of largest island of 1s.

Enhancing expression levels using SCP3 promoter

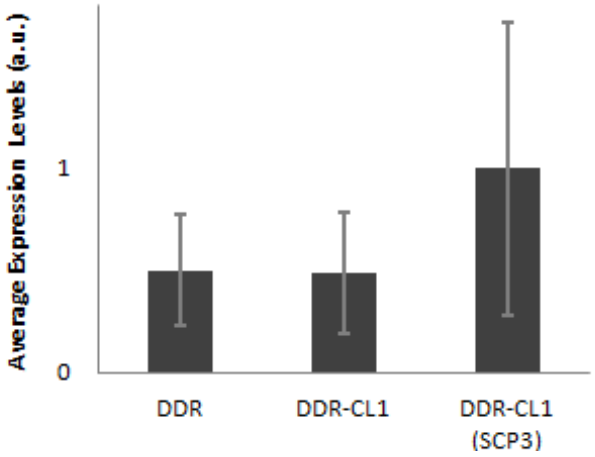

Figure S2. Related to Figure 3. Average expression levels of cells expressing DDR or DDR-CL1 under a CMV promoter compared to cells expressing DDR-CL1 under a SCP3 promoter. Expression levels were measured by using a confocal microscope with a 60x objective to first acquire the images, then suing MATLAB individual cells expressing CMV-DDR, CMV-DDR-CL1 and SCP3-DDR-CL1 were identified and segmented (n=29-56). After segmentation, the average total intensities were calculated by integrating each specific ROI and normalizing by the ROI size. The distributions of average expression levels of DDR-CL1 were compared using the Mann-Whitney U test, which enabled us to reject the null hypothesis that expression levels were the same using the two promoters (P-value = 0.002).

Table S1. Related to Figure 4. Simulation parameters of PIPE tests and artifacts investigation

Purpose	Random walk type	Step size variance (px^2)	Fraction of subpopulations	Mean emission (photons / time step)	Expected α	Output α (10 replicates)
Test PIPE	Classical	[0.0001,0.01]	--	400	1	1.00±0.01
	CTRW	0.0015 0.003 0.006	--	400	0.8	0.26±0.01 0.42±0.01 0.55±0.01
	CTRW	0.0015 0.003 0.006	--	400	0.6	0.14±0.01 0.32±0.01 0.43±0.01
Population heterogeneity	Classical	0.001 / 0.001 0.001 / 0.002 0.001 / 0.003 0.001 / 0.004 0.001 / 0.005	0.5 / 0.5	400	1	1.00±0.02 0.76±0.01 0.53±0.01 0.46±0.01 0.46±0.06
	Classical	0.001 / 0.002	0 / 1 0.1 / 0.9 0.2 / 0.8 0.3 / 0.7 0.4 / 0.6 0.5 / 0.5 0.6 / 0.4 0.7 / 0.3 0.8 / 0.2 0.9 / 0.1 1 / 0	400	1	0.99±0.01 0.75±0.10 0.85±0.03 0.91±0.03 0.89±0.04 0.91±0.1 0.94±0.03 0.98±0.03 0.98±0.04 0.99±0.03 0.99±0.02
Noise floor threshold	Classical	0.005	--	200 300 400 500	1	See Fig. S3C

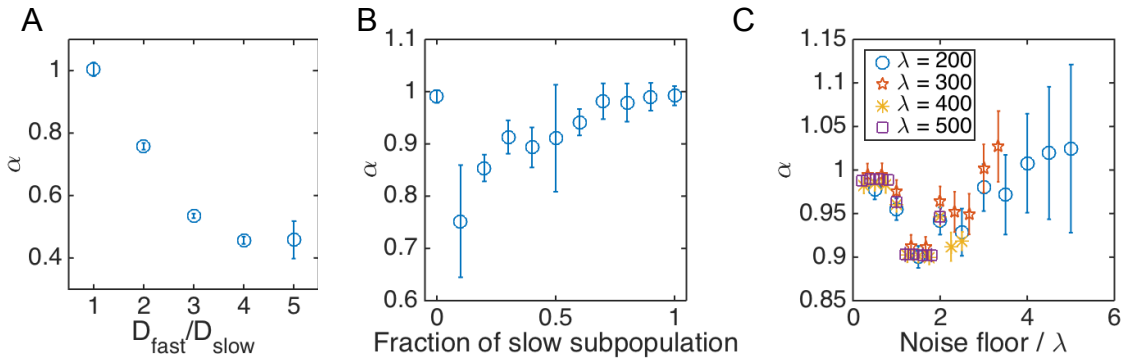

Figure S3. Related to Figure 4. Effect of potential artifacts on PIPE's calculation of α. A) Simulations of random walk with two equal particle populations, each with a different diffusion coefficient. α is shown as a function of the ratio of the diffusion coefficients. D_{slow} was held constant, as a variance of step size distribution of $0.1px^2$. B) Simulations of random walk of two particle populations with diffusion coefficient ratio of 2 (step size variances of $0.1px^2$ and $0.2px^2$). α is shown as a function of the relative fraction of the slow population. C) Simulations of random walk with a single population were processed using a noise floor threshold, below which the signal vanishes. α is shown as a function of the noise floor threshold, in units of the mean emission λ of a single particle. Several values of λ were simulated, and all the curves collapse into a similar trend upon normalization of the noise floor. All errorbars represent the mean and s.e. of 10 replicate simulations.

Supplemental methods

PIPE theory and data analysis

PIPE's theory and computational analysis consist of filtering the signal from the raw imaging data and fitting it to an expanding Gaussian. We designed the computational analysis to work under a wide range of measurement noises and signal strengths, using a dynamic signal averaging scheme. The stages of the computational analysis are described in detail below. PIPE's user manual and the entire source code can be found at englandlab.com.

Image segmentation

A typical photo-conversion movie shows a single cell, which may of may not fill the entire field of view. Excluding the cell exterior from the analysis is a crucial feature of the data analysis for two reasons, both of which are related to the subsequent Gaussian fitting of the intensity profiles. The first reason to exclude the cell exterior from the data analysis is that the cell interior emits more fluorescence than the cell exterior, which means that intensity profiles that pass through the cell membrane can be reasonably fitted to Gaussians even after the profiles stop expanding and reach steady-state. Because intensity profiles that are solutions to the diffusion equation need to be flat at steady-state, the fluorescence contrast created by the cell exterior would lead to incorrect Gaussian fits. The second reason to exclude the cell exterior from the data analysis is that when the intensity profiles reach the cell boundary, the main assumptions of PIPE break down: the MSD stops growing linearly with time, and the intensity profile shape deviates from a Gaussian.

To exclude the extracellular space from the analysis, it is straightforward to use standard image segmentation algorithms. We used the following algorithm (see Fig. S1 for output of different stages):

1) *averaged_image = average_pixel_by_pixel(first 30 images of movie)*
2) *edge_mask = detect_edges(averaged_image)* % sharp spatial fluctuations in brightness are identified as edges and marked as 1s while other pixels are marked as 0s.
3) *dilated_mask = dilate(edge_mask)* % edge detection may not identify the whole cell membrane, so dilation helps filling gaps in the segmented membrane and create a continuous stretch of 1s.
4) *filled_mask = fill_holes(dilated_mask)* % creates islands of 1s in a sea of 0s
5) *eroded_mask = erode(filled_mask)* % shaves off some 1s from the island perimeters to compensate for the dilation in step (3)
6) *cell_mask = find_largest_island_of_1s(eroded_mask)* % identify the cell as the largest island of pixels with value 1. This compensates for background noise that may cause the edge detection algorithm to segment other edges that are outside the cell.

Note that this algorithm creates a cell mask based on the first 30 images of the movie, and assumes that this mask describes the cell interior during the entire movie. This assumption is justified, since we did not observe any cell motility during the imaging time. In addition, we only considered the cell boundary to appear in the field of view if the area taken by the cell interior was less than 90% of the field of view area. Otherwise, no cell was detected, and the cell mask included the entire field of view. We made this choice because our algorithm often detected artificial boundaries very close to the borders of the field of view, even in *in vitro* data, where no cells are imaged.

Automatic detection of pulse coordinates

PIPE only analyzes the frames acquired after the photo-converting laser has turned off. In addition, PIPE defines the intensity profiles so that they pass through the center of the photo-converted ensemble, where the fluorescence intensity is highest. To achieve these restrictions, PIPE automatically identifies the coordinates of the pulse, i.e. the frame where the photo-conversion laser was turned off and the pixel that marks the center of the fluorescence at that frame. While this task can be done manually by the end-users, automating it makes it easier to apply PIPE to a large number of movies. We used the following procedure:

1) *for t=0:end*
    a. *total_fluorescence(t) = average_within_image(movie(t))*
2) *t_start = detect_sudden_change_in_gradient(total_fluorescence)*

3) *t_end_of_pulse=find_location_of_peak(total_fluorescence(t_start:end))* % the photo-conversion laser increases the average fluorescence in the field of view, so the frame that contains the highest average fluorescence after t_start is the last frame before the laser was turned off.
4) *area_of_pulse = segment_image(movie(t_end_of_pulse))* % this image segmentation is similar to the procedure used in the previous section, only that instead of edge detection we use thresholding on T percent of maximum fluorescence. We start from T=100% and gradually lower T until the detected area has a radius between 15 and 100 pixels. (The entire field of view is 512 pixels wide).
5) *[x_center, y_center] = find_centroid(area_of_pulse)*

Correction of baseline fluorescence and noise reduction

To eliminate background fluorescence from the analysis, data acquired prior to the pulse was averaged-over, smoothed and then subtracted from the rest of the data. Next, measurement noise was decreased by averaging images at consecutive time points pixel-by-pixel, and assigning to the resulting image a single time point at the middle of the averaged-over time range. The averaging scheme (number of images averaged at each time point) was designed to keep the SNR high for a long time while avoiding averaging too much and thereby distorting the Gaussian shape of the intensity profiles. Lastly, one-dimensional intensity profiles were segmented from the images in the horizontal dimension. The profiles were averaged over several parallel lines (usually 30) pixel-by-pixel to further decrease noise.

Random walk simulations

To test how PIPE's accuracy is affected by various types of noise and potential artifacts, we imitated imaging data by simulating diffusion starting from a Gaussian initial condition. It is well known in statistical mechanics that Fickian diffusion emerges from a large number of particles undergoing random walks. In this section we describe our simulations, in which we generated trajectories of random walkers and then binned the trajectory data into pixel matrices.

Core random walk algorithm

The simplest random walk algorithm is well known: starting from time zero and any initial locations, at each time step every simulated particle takes a spatial step of constant size either left or right in every spatial dimension. This simple algorithm generates trajectory ensembles with two important properties: $\langle \vec{x} \rangle = 0$ and $\langle |\vec{x}|^2 \rangle = 2dDt$, where $\vec{x}$ is displacement and triangular brackets denote ensemble average, and where d is the number of spatial dimensions, t is the time step and D is the effective diffusion coefficient of the ensemble. D is not an input parameter of the algorithm, but a result of the similar behavior of many random walkers and a continuous concentration following the diffusion equation.

We slightly modified this basic algorithm by sampling the step sizes from a continuous normal distribution with mean 0, instead of randomizing between +1 and -1. This choice does not change the properties above. We chose to switch to this distribution because the only variable in this distribution is the variance, which is linear in D. Thus, by changing the step size distribution we directly change D and only D. In addition, this continuous distribution allowed us to work with a continuous space rather than with a discrete space, which removes finite-size effects that exist when working with discrete spaces.

We chose the simulation parameters to most accurately imitate the real microscopy data. We considered the unit of each time step to be $10ms$ and the unit of the step size variance to be $1\mu m^2$. We explored three orders of magnitude of step size variance, from 0.001 to 2, which correspond to diffusion coefficients between ~$0.1\mu m^2/sec$ and ~$200\mu m^2/sec$. This range covers most of the biomolecules in the cell, from large organelles and membrane proteins to small peptides in the cytoplasm. We sampled the initial locations of the particles from a two-dimensional normal distribution with standard deviation of $3\mu m$, similar to the observed photo-converted proteins in our experiments immediately after the photo-conversion pulse. We chose the number of particles to be 10^5, which fits the expected number of photo-converted fluorophores in a typical experiment: according to bionumbers.hms.harvard.edu, there are ~10^{10} proteins in a mammalian cell, which corresponds to a concentration of ~$10^8 proteins/(\mu m)^3$. Highly expressed proteins comprise ~1% of cellular proteins or less, so in our experiments, DDR concentration is at most $10^6 proteins/(\mu m)^3$. The photo-conversion pulse converts a volume of ~$(\mu m)^3$, and assuming 10% conversion efficiency, we obtain 10^5 photo-converted proteins. We simulated each particle for 1000 time steps, matching a typical experiment of 10 seconds.

We chose to perform the simulations in two spatial dimensions, because this way we struck a balance between the aims of accurately imitating our experiments and keeping simulation time feasibly short. Since our COS7 cells are much wider than they are thick, and since the focal plane contains most of the cell volume in the height dimension, the cell's interior can be approximated as a two-dimensional space. A more precise model would include the third dimension and would use various shapes to imitate the cell membrane in the third dimension, but the additional accuracy of this model would come at a significant expense in time dedicated to checking the effects of the cell shape on the results. Even in thick *in vitro* samples, diffusion is effectively two-dimensional, because the concentration profile at $t = 0$ is only Gaussian in the horizontal dimensions. In the vertical dimension fluorescence can be approximated as uniform, since the photo-conversion laser passes through the whole sample in the vertical dimension.

Before running PIPE on the simulated data, we tested a few simulations (chosen at random) for the behavior of the mean displacement and the MSD. We directly calculated the displacement and MSD, averaged over the trajectory ensemble at each time point. We then calculated the time average of the mean displacement and found that it is very close to zero (i.e. much smaller than a typical step size), as expected. In addition, we fitted MSD versus time to a power-law and obtained an exponent of 1±0.02, verifying the expected linear temporal scaling.

Simulation of Continuous Time Random Walk (CTRW)

As mentioned above, we simulated normal diffusion by sampling random spatial steps from a (Gaussian) probability distribution, while leaving the waiting times between steps constant. Here, we simulated CTRW by random sampling of both the spatial steps and the waiting times. To obtain anomalous diffusion from CTRW, we sampled the waiting times from a power-law distribution $P(t) \propto 1/t^{1+\alpha_{sim}}$, where α_{sim} is the desired anomalous exponent (Metzler and Klafter, 2000).

Pre-processing of simulated data

To match the format of the simulated data to that of our imaging data, we processed the simulated trajectory information into a time series of pixel matrices. First, we created a virtual field of view by choosing a cutoff distance of 30μm (with one exception, described in the Results section in the main text, where we explored cutoff distances between 3-45μm). The cutoff distance of 30μm corresponds to the edge of the field of view at maximal zoom in our imaging system. We placed the photo-converted particles in the middle of the frame by ignoring particle locations that were half of the cutoff distance away, in either x or y direction, from the center of the initial distribution. Then, we binned the location information into pixels by dividing the field of view to equal squares and counting the number of particles within each square at every time point. We chose the square size so that we would end up with 512 pixels in each dimension, mimicking our imaging data.

Noise addition

Our random walk simulations were a useful tool for exploring how noise affects PIPE's output. We introduced two types of noise to the data. First, we added Poissonian shot noise, which was intended to capture the variability in number of photons detected from the fluorophores due to the stochastic nature of fluorophore excitation and emission. We implemented this noise by mapping each pixel value, from the number of fluorophores in the pixel (N) to fluorescence intensity value. The mapping procedure included sampling N times from a Poisson distribution with average λ. We usually chose λ to be 400, which corresponds to the expected number of excitations of a single fluorophore during an acquisition time of a diffraction limited spot on our imaging system (~1μs at maximal zoom), given the decay time of GFP (2.6nsec) (Swaminathan et al., 1997). The accuracy of PIPE (average error in the EDC) did not change when we chose different values of λ between 1 and 1600. The second type of noise we added was background noise, which was aimed to represent autofluorescence and imaging-system-noise (e.g. dark current). To generate this noise, we added to each pixel at each time step a value that we sampled from a Poisson distribution with mean value 500. Using other mean values for this distribution, between 100 and 1900, did not change PIPE's accuracy.

Photo-bleaching

We added uniform photo-bleaching to the simulations in the form of stochastic and irreversible switching off of single particles with a constant probability rate. This stage took place in the trajectory generation phase, before pre-processing and noise addition. We implemented photo-bleaching by choosing a bleaching rate ω and sampling once

from a uniform distribution between 0 and 1 for each particle at each time step. If the number we sampled was less than ω, we considered the particle bleached, and stopped sampling time steps for that particle until the end of the simulation. We tried ω values of 10^{-1}, 10^{-2}, 10^{-3} and 10^{-4}. The only case where bleaching significantly perturbed PIPE's output was the case where $\omega = 10^{-1}$. Further details about the effect of simulated photo-bleaching rates are elaborated in the Results section below.

Artifact exploration

When performing simulations of anomalous diffusion, and when measuring the anomalous exponents of purified proteins *in vitro*, PIPE measured α-values that differed from the expected anomalous exponents, i.e. the simulated anomalous exponents α_{sim} in the simulations and $\alpha = 1$ in solution, which describes the normal diffusion that takes place there. To explain this discrepancy between measurement and expectation, we screened an array of possible artifacts and found that population heterogeneity and non-linear fluorescence detection might skew the computational analysis. To examine the effect of population heterogeneity, we simulated normal diffusion with two subpopulations of random walkers, each with a different diffusion coefficient, and analyzed their motion with PIPE. The results we obtained showed that α is indeed smaller than 1, and that it decreases as the gap between the diffusion coefficients of the subpopulations widens (Fig. S3A). In addition, α decreases as the fraction of the slower subpopulation decreases (Fig. S3B). This behavior is not expected from the MSD, whose temporal scaling remains linear even when subpopulations vary in their diffusion coefficients. The probable explanation for our unexpected result is that the intensity profile of a heterogeneous population does not remain Gaussian under the diffusion equation. This means that the width of the profile's Gaussian fit is not always linearly proportional to the MSD, and can therefore scale differently with time, i.e. with unexpected values of α. To check whether heterogeneity in oligomerization state is the cause for observing $\alpha < 1$ *in vitro*, we measured α under a 100-fold range of DDR concentrations, and observed no change in α. This finding suggests oligomerization does not artifactually affect α, because such a significant change in concentration should modulate the relative abundance of monomeric and dimeric DDR (Fron et al., 2013). Nevertheless, we cannot rule out population heterogeneity as an artifact, for example concentration-independent heterogeneity, which might arise from DDR binding to side-products of the purification.

Another effect that might cause the downward shift in measuring α is non-linear fluorescence detection. To examine this effect, we changed the way simulated data is processed so that every pixel with fluorescence intensity below a threshold ("noise floor") was assigned a value of zero, while pixels with values above the threshold remained unchanged. We performed this procedure under a range of emission statistics (changing the mean λ of the Poissonian fluorescence emission for the simulated particles) and found a persistent decreasing trend of α from 1 to 0.9 as the noise floor increases from zero to 2λ. Beyond 2λ we identified no trend, as α values fluctuated significantly between replicate simulations (Fig S3C; See Table S1 for parameter values used in each simulation and for numerical results). While it is plausible that imaging systems have lower bounds on detection sensitivity, it is challenging to verify whether a noise floor as low as 2λ really exists. A signal of 2λ correponds to a concentration of ~2 fluorophores per pixel on average. In such low concentrations, the actual number of fluorophores per pixel fluctuates dramatically, so a non-zero average signal is expected even if no signal is registered from pixels with two fluorophores or fewer. It may be possible to test the noise floor hypothesis using immobile fluorophores, ideally of the kind that does not photo-bleach.

Differences between *in vitro* and *in vivo* data

One of our main claims in this work is that choosing to use EDCs to describe protein motion enabled us to validate PIPE *in vitro*, where protein motion can be justifiably modeled as Fickian diffusion. Obtaining accurate results *in vitro* allowed us to assert that results such as cell-to-cell variability in EDCs describe real biophysical differences, rather than flaws in PIPE. To reach this conclusion, it is necessary to establish that the *in vitro* and *in vivo* data are sufficiently similar in all aspects other than the underlying physical process.

While the *in vitro* and *in vivo* data share many properties because they were acquired by the same imaging system, they differ in their time durations. While *in vitro* movies were analyzable up to one hundred frames after photo-conversion, *in vivo* movies were usually analyzable only up to frame number 10 or 20. The frames that followed were too noisy to analyze: they produced Gaussian fits with low amplitudes compared with the magnitude of noise, and with widths that had large error bars and that broke the trend of linear scaling of the square widths from the first 10 or 20 frames. To understand the effect of the movie duration on the accuracy of measuring the EDC, we reanalyzed all the *in vitro* movies only up to frame 15, and we found that as a result, the EDC increases by 21%±17% on average pulse or minus one standard deviation. This finding decreases the expected accuracy but does not undermine the applicability of PIPE *in vivo*.

Supplemental references

Fron, E., Van der Auweraer, M., Moeyaert, B., Michiels, J., Mizuno, H., Hofkens, J., and Adam, V. (2013). Revealing the Excited-State Dynamics of the Fluorescent Protein Dendra2. J. Phys. Chem. B *117*, 2300–2313.

Metzler, R., and Klafter, J. (2000). The random walk's guide to anomalous diffusion: a fractional dynamics approach. Phys. Rep. *339*, 1–77.

Swaminathan, R., Hoang, C.P., and Verkman, A.S. (1997). Photobleaching recovery and anisotropy decay of green fluorescent protein GFP-S65T in solution and cells: cytoplasmic viscosity probed by green fluorescent protein translational and rotational diffusion. Biophys. J. *72*, 1900–1907.